Dielectric response of a dipolar molecular rotor crystal

Robert D. Horansky, Laura I. Clarke,* and John C. Price
Department of Physics, 390 UCB, University of Colorado, Boulder, Colorado 80309-0390, USA

Tinh-Alfredo V. Khuong, Peter D. Jarowski, and Miguel A. Garcia-Garibay
Department of Chemistry and Biochemistry, University of California, Los Angeles, California 90095-1569, USA
(Received 9 July 2004; revised manuscript received 12 August 2004; published 6 July 2005)

We report the results of the dynamics of a three dimensional lattice of dipolar molecular rotors where the unit cells consist of a dipolar phenylene ring rotating about an axle stabilized by stationary triphenyl groups. The molecules are synthesized such that the lattice may be customized to elicit novel and useful physical phenomena. Using dielectric spectroscopy and ^{2}H NMR, we demonstrate rapid thermal rotation of the molecular rotors in the solid state, and characterize the depth and asymmetry of the rotational potential. Calculations show that rotor-rotor interactions are weak in this structure, and the rotational potential is dominated by steric interactions between each rotary element and the nonrotating portions of neighboring molecules.

DOI: 10.1103/PhysRevB.72.014302 PACS number(s): 77.22.Gm, 77.84.−s, 81.07.−b, 81.07.Nb

The potential of controlling dielectric and phonon phenomena in ordered arrays of well-designed molecular dipolar rotors has been recognized for some time.[1–5] Ferroelectric and antiferroelectric phases are expected, with polar rotary phonons propagating at velocities that are lower than those typical of sound waves in conventional condensed media.[5] Goldstone modes are also predicted in two dimensional (2D), square and triangular lattices.[1] Although rotating groups are common in polymers[6] and several other solid systems,[7,8] there are no examples of three-dimensional (3D) crystal lattices of synthesized dipolar rotors.[7,9] However, the rapidly developing field of crystal design is opening paths to realizing materials with unique solid-state properties,[9–14] while at the same time synthesized molecular rotors have received attention as a fundamental element of nanotechnology.[7,15–20] Combining these avenues, in this paper we describe crystals of a polar phenylene rotor and characterize its dynamics by both NMR and dielectric spectroscopy. Features of the rotational potential derived from dynamic measurements were confirmed by variable temperature single crystal x-ray diffraction and a force field computational model. Our approach to the creation of ordered polar rotor arrays allows control over the rigid super structure, the axle of rotation, the size and dipole moment of the rotating group, and the spacing of the dipoles, thus providing a tunable solid state system.

The molecule of interest is shown in Fig. 1(a) with a space-filling model and line structure of 1,4-bis(3,3,3-triphenylpropynyl)-2-fluorobenzene,[21] henceforth referred to as ROT-F. The rotating part (shown in red) consists of a phenylene group with a fluorine atom that imparts a permanent electric dipole moment to this assembly of 1.5 D. The triple bonds constitute the linear axle that permits rotation along an essentially barrierless gas phase potential and the two bulky triphenylmethyl groups (in blue) help reduce the packing density around the rotor to minimize steric hindrance in the crystal. This design may be used as a prototype for future molecules with variation of the dipole moment of the rotating group or size of the bulky stationary group.

Variable temperature nuclear magnetic resonance studies of ROT-H, the nonpolar analog of ROT-F with hydrogen in lieu of fluorine, have shown exchange among two degenerate positions related by a 180° flip with a rate of ~15 kHz at 298 K.[20] Knowing that hydrogen and fluorine have similar volumes, we expect ROT-H and ROT-F to have isomorphous crystal structures with similar rotational dynamics. In fact, two crystal structures of ROT-F are obtained by slow evaporation of benzene or dichloromethane solutions and allow more control over the rotor dynamics. Both crystal structures are isomorphous with those previously determined for ROT-H. These are a benzene-containing clathrate and a solvent-free structure, both belonging to the space group $P\bar{1}$. Although the addition of the fluorine atom to make ROT-F reduces the molecular symmetry of ROT-H from *Ci* to *C*1, x-ray diffraction analysis at 100 K showed that the space group symmetry in ROT-F is satisfied by disorder of the fluorine atom over two positions related by the crystallographic inversion center.[21] With respect to the flipping motion observed in ROT-H, an important consequence of the fluorine atom substitution is that rotation of the fluorophenylene group is no longer degenerate and occurs over an asymmetric potential with one of the two sites preferred by the fluorine atom over the other as illustrated in Fig. 1(b).

In order to investigate the rotary motion of ROT-F with dielectric spectroscopy, we use interdigitated surface capacitors on fused silica with gold thin-film electrodes.[15] Each device has 25 electrode finger pairs, 1 mm in length, 200 nm thick, and with 10 μm gaps between digits. Samples are prepared by drop casting saturated ROT-F dichloromethane or benzene solutions onto the electrodes to yield three dimensional polycrystalline structures over and between the interdigitated fingers of the device. In these experiments, the rotational dynamics of the dipolar rotors is tuned as a function of temperature from 80 to 370 K and probed by measuring their response to an external ac electric field at three fixed frequencies of 0.1, 1, and 10 kHz. The scan over our experimentally accessible temperature range provides access to ro-

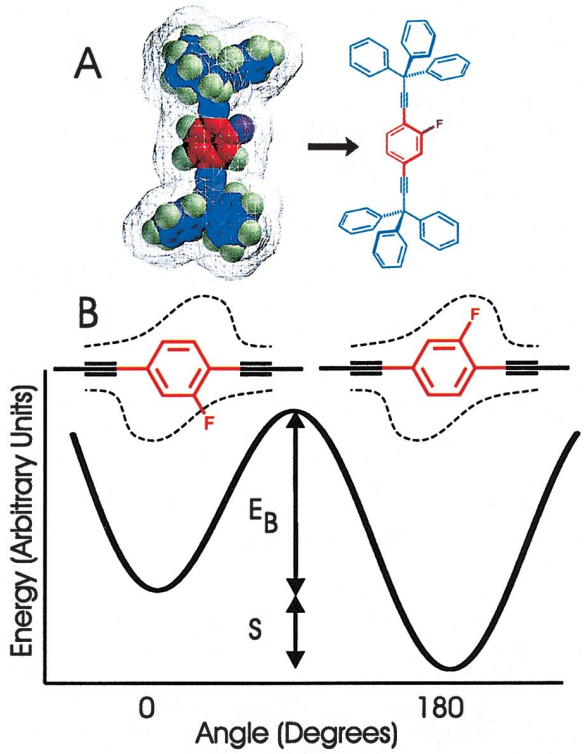

FIG. 1. (Color) The top figure (a) is the chemical structure of 1,4-bis(3,3,3-triphenylpropynyl)-2-fluorobenzene shown in a space-filling model with a surface of 2.4 Å representing the van der Waals boundary of H atom contacts (left), and with a line structure highlighting the fluorine atom and the triple bonds (right). The rotor assemblies are shown in red and the static segments in blue. In the bottom frame (b) is an idealized rotational potential with the corresponding molecular configuration shown above each potential minimum. The dashed lines around the rotary units represent the cage-like environment that hinders rotation.

tor dynamics at rates from less than millihertz to gigahertz in a single measurement apparatus. The alternative approach of scanning the measurement frequency over such a large range would require several measurement techniques and would limit the precision of the dielectric measurements. A peak in the dielectric loss, or $\tan(\delta)$, of the rotors in the surface capacitor is found for both desolvated and clathrate crystals of ROT-F as shown in Figs. 2(a) and 2(b), respectively. The signal of the clathrate structure is broader and of lower magnitude than that from the desolvated structure. To check that the signal seen is due to the dipolar rotary portions and not the substrate or bulk crystal, the same experimental procedures were performed on the nonpolar analog, ROT-H, with the measurement showing no structure relative to the blank electrode.

Based on previous dynamics measurements on nonpolar ROT-H, we explain the dielectric data in terms of a model that involves thermal hopping of the central dipole between the wells of a twofold rotational potential. The polarization relaxation rate, $1/\tau$, will be dominated by the fastest hopping rate and is given by

$$\frac{1}{\tau} = \omega_0 \exp\left(\frac{-E_B}{kT}\right), \tag{1}$$

where E_B is defined in Fig. 1(b), ω_0 is the attempt frequency (or libration frequency of the rotor in the well), and k is Boltzmann's constant.

If we suppose that the system is lossless except for the effects of rotor motion, then we may represent the dielectric loss as

$$\tan(\delta) = \frac{C_R}{C_0}\frac{\omega\tau}{1+\omega^2\tau^2}, \tag{2}$$

where ω is the measurement frequency and $1/\tau$ is the relaxation rate with the temperature dependence given by Eq. (1). In this expression, C_0 is the lossless capacitance of the sample due to everything except the rotary elements, namely the substrate and the nonrotary portion of the molecular crystal. C_0 is typically near 1 pF. The factor C_R is the static capacitance contributed by the dipole rotors. An explicit expression for C_R can be given for an idealized situation: a parallel plate capacitor with area L^2 and gap L, completely filled with a homogenous dielectric material containing the polar rotors

$$C_R = \frac{\epsilon_R + 2}{3}\frac{Np_0^2}{3kTL^2}\cosh^{-2}\left(\frac{S}{2kT}\right). \tag{3}$$

The total number of rotors in the capacitor is N, and the bare dipole moment is p_0. The rotors are assumed noninteracting and located in spherical cavities in the dielectric medium, where $\epsilon_R \approx 2$ is the dielectric constant of the medium, leading to the local field correction factor $(\epsilon_R+2)/3$.[22] The $\cosh^{-2}$ term is a suppression factor accounting for the freezing of rotors in the lower well as the temperature decreases.[23] The well asymmetry, S, is shown in Fig. 1(b). Except for an overall numerical factor of order unity, which is not important for our purposes, we expect Eq. (3) to apply to the present data if we set L equal to the 10 μm gap. The value of N estimated for our samples from the geometry and crystal density is 5×10^{15}.

E_B and ω_0 are extracted from an Arrhenius plot. According to Eq. (2), a peak in $\tan(\delta)$ occurs at a temperature T_{peak} where the measurement frequency ω is equal to the relaxation rate, $1/\tau$. A plot of $\ln(\omega)$ vs $1/T_{peak}$ should then give, according to Eq. (1), a straight line with a slope equal to E_B and a y intercept of $\ln(\omega_0)$. The plotted data points are shown in the bottom right portion in Fig. 2(d) along with a linear fit. Both the dichloromethane and benzene crystallized samples yield the same Arrhenius plot with barriers to rotation of 13.7 ± 0.9 kcal/mol. As is often found, the experimentally seen attempt frequency $\omega_0=6\pm5\times10^{14}$ s^{-1} is much larger than the libration frequency of 8.5×10^{12} s^{-1} estimated from the moment of inertia and barrier height. This implies that there is a small linear temperature dependence of the barrier height of -8×10^{-3} kcal/mol K.

Using E_B and ω_0 from the Arrhenius plot, the experimental $\tan(\delta)$ line shape can be fit using Eq. (2) with C_R substituted from Eq. (3). Figure 2(a) shows the fits to the dichloromethane data using Eq. (2) with the well asymmetry S and

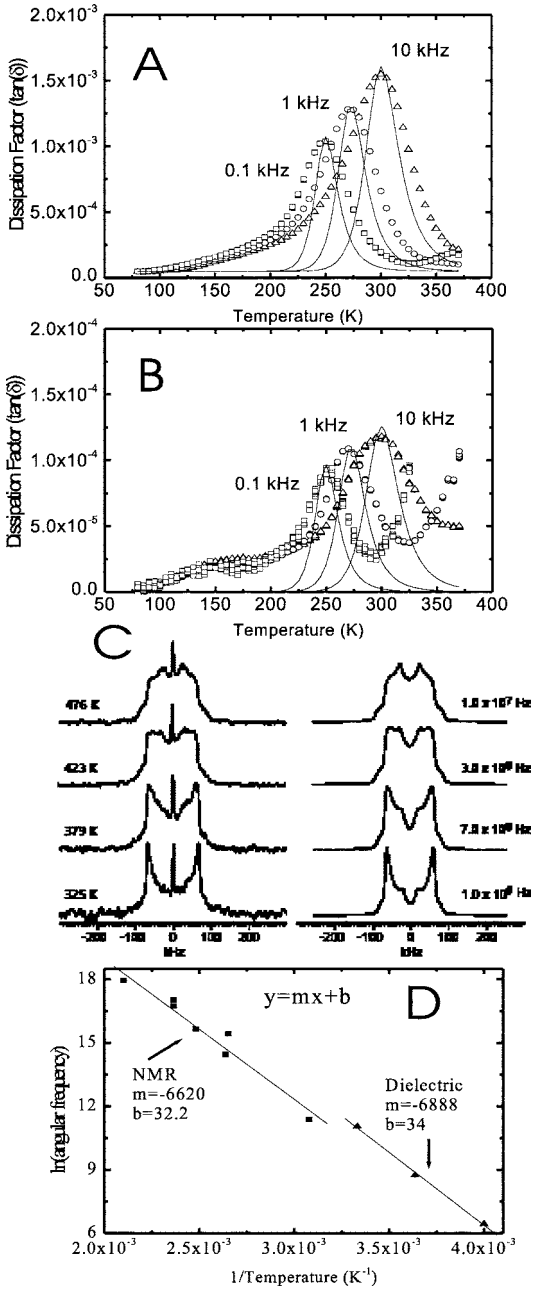

FIG. 2. Experimental data. The top two plots are temperature scans of tan(δ) for the desolvated dipole rotor (a) and clathrate (b). The open symbols represent the data with the background subtracted for measurements at 100 Hz (open squares), 1 kHz (open circles), and 10 kHz (open triangles). The solid lines are fits to each frequency using Eq. (2) with a barrier of 13.7 kcal/mol and asymmetry of 1.9 and 1.5 kcal/mol for desolvated and clathrate, respectively. Another measure of the rotary potential parameters is the ^{2}H NMR data (c). Data on the left correspond to measurements at various temperatures (shown next to each plot). The peak in the center of the spectra corresponds to isotropic motion experienced by a relatively small percentage of deuterated molecules adsorbed onto the glass surface of the sample holder. The plots on the right show fits to the data on the left using the frequencies shown next to each plot and populations in the two potential wells corresponding to an asymmetry of 0.78 kcal/mol. Arrhenius plots derived from NMR and dielectric data are shown in (d).

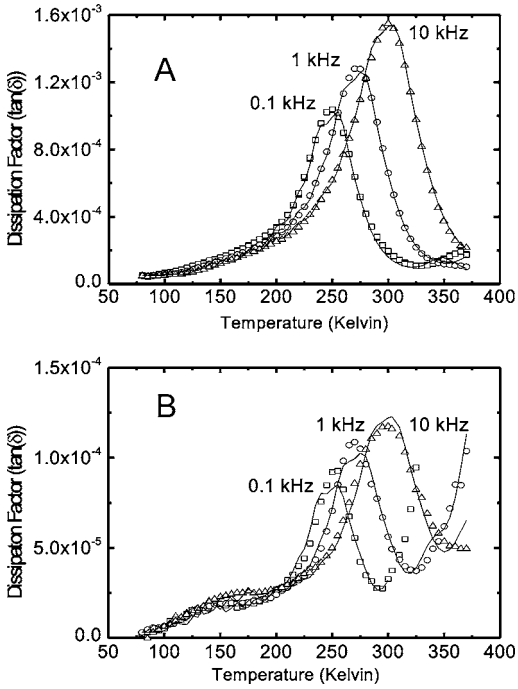

FIG. 3. Theoretical multi-peak fit to dielectric data of ROT-F in desolvated crystal (a) and clathrate (b). The open symbols in both plots show the dielectric loss versus temperature with the background from a blank electrode subtracted for measurements at 100 Hz (open squares), 1 kHz (open circles), and 10 kHz (open triangles). The solid lines are fits to each frequency using Eq. (2) with a sum of loss peaks ranging from 5 to 19 kcal/mol with 1 kcal/mol spacing and the number of active rotors altered to fit. The asymmetry is set to be linearly varying from 0 kcal/mol asymmetry at 0 kcal/mol barrier to 1.9 or 1.5 kcal/mol asymmetry at a barrier of 13.7 kcal/mol for the desolvated (a) and the clathrate (b), respectively.

overall magnitude, dictated by the number of contributing rotors N, left as adjustable parameters. With these free parameters fit concurrently to data at all three frequencies, a unique well separation of 1.9 ± 0.2 kcal/mol for the desolvated sample and 1.5 ± 0.2 kcal/mol for the clathrate structure were obtained. The number of contributing rotors in the desolvated case is 1.7×10^{15}, which agrees well with our estimate of $N=5\times10^{15}$ based on sample geometry.

The fitted single Debye peaks are too narrow to account for the full peaks seen, which may be due to the presence of rotors in different local environments. By fitting the whole spectrum with a multitude of barrier heights with 1 kcal/mol spacing between 5 and 19 kcal/mol and asymmetry varying linearly with barrier height, the theoretical peak shown with a solid line in Fig. 3(a) is found. Based on summing the magnitudes of rotors used in each peak to create the broad fit, we estimate the single Debye relaxation model accounts for about 2/3 of the active rotors in the desolvated crystal. The same technique is used for the clathrate crystal, shown in Fig. 3(b), with an alteration in the slope of the linearly varying asymmetry which is chosen to be 1.5 kcal/mol in this case at 13.7 kcal/mol barrier. The single Debye model accounts for about 1/2 of the active rotors for the clathrate. The differences seen in the clathrate from the desolvated

crystal, namely broader peaks and lower asymmetry, may be due to a wider range of barriers caused by benzene evaporation and structural changes due to temperature cycling.

The barrier to rotation, attempt frequency, and asymmetry are also accessible through ^{2}H NMR spectroscopy[24] of an analog of ROT-F with all the hydrogens in the central rotor exchanged by deuterons. The method relies on the analysis of spectral changes caused by dynamic averaging of the orientation-dependent interaction between the ^{2}H nuclear electric quadrupolar moment and the electric field gradient (EFG) at the nuclear position. Representative examples of spectra taken with static powder samples made from single crystals of ROT-F are shown on the left in Fig. 2(c). Each deuteron gives a doublet of peaks with a splitting frequency

$$\nu = D_n \cos^2 \beta, \tag{4}$$

where

$$D_n = \tfrac{3}{4} Q_{CC}(3 \cos 2\beta - 1). \tag{5}$$

Q_{CC} is the quadrupolar coupling constant (180 kHz for aromatic deuterons),[29] and β is the orientation angle of the C—H bonds with respect to the external magnetic field. An isotropic distribution of aromatic C—H bonds in a static polycrystalline sample results in a typical powder pattern (Pake pattern), characterized by symmetric discontinuities due to the C—^{2}H bonds that are parallel or perpendicular to the external field. Variations in the powder pattern caused by deuteron exchange among magnetically nonequivalent sites depend both on the exchange frequency and on changes in population between exchanging sites. All spectra were obtained on a Bruker DSX-300 NMR spectrometer operating at a ^{2}H frequency of 46.05 MHz equipped with a 5 mm solenoid coil. Measurements were carried out between 295 and 425 K and the temperature was calibrated using ^{195}Pb shift standard. Spectra were acquired with a quadrupolar echo sequence using a 90° pulse of 2.25 μs followed by dephasing and refocusing delays of 40 and 50 μs, respectively. The spectra shown in Fig. 2(c) were processed with a line broadening of 2.0 kHz to reduce noise, and subsequently simulated using the program reported by Nishikiori *et al.*[25] with a model that involves exchange between two sites related by 180° rotation and using the rate constants and population values that best reproduce the experimental results. The rates and their corresponding temperatures are plotted in Arrhenius format, shown in Fig. 2(d), from which the barrier and attempt frequency are found. The fit in Fig. 2(d) to the NMR data yields a barrier to rotation of 13 ± 2 kcal/mol and an attempt frequency of $1.0 \pm 0.7 \times 10^{14}$ s^{-1}. The population ratios correspond to an asymmetry of 0.78 ± 0.05 kcal/mol.

While dielectric and ^{2}H NMR spectroscopy agree with respect to the barrier to rotation and the presence of an asymmetry, the magnitude of the latter is in disagreement. In search of an independent measure, a single crystal x-ray diffraction structure of ROT-F was solved with data taken at 296 K. The temperature dependence of the equilibrium population of the fluorine atom is reflected in a splitting of its electron density over two nonequivalent sites. Single crystal data yielded a population ratio in the higher energy well of 1:4 corresponding to an asymmetry of 0.7 kcal/mol, corroborating the NMR results. The reason for the discrepancy between dielectric results and the results of NMR and x-ray may lie in the structure of the material being measured. The dielectric measurements are performed on polycrystalline material made from rapid evaporation while x-ray and NMR experiments measure single crystals and polycrystalline samples grown by slow evaporation from solution. While the local environments of these two structures must be very similar, since they yield the same barrier heights, there may be small differences that could account for the 1 kcal/mol asymmetry difference.

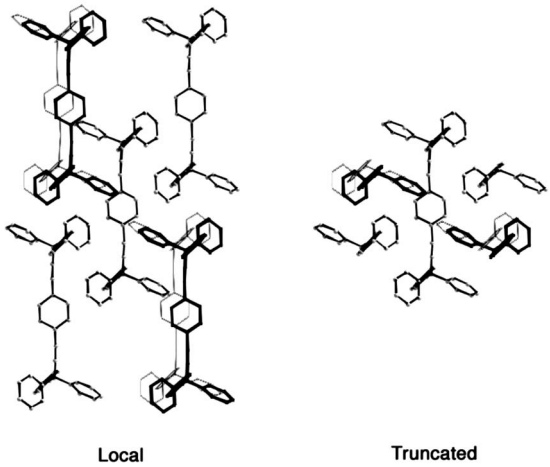

FIG. 4. Local and truncated models used to investigate the rotational potential energy surface of both (1) and (2) (fluorine not shown). Dark rotors are in front and light rotors are behind.

In addition to our experimental findings, we calculate the rotational potential for both polar ROT-F and ROT-H in their desolvated configurations using the molecular mechanics force field MM3* as implemented by the program Macromodel.[26,27] Since ROT-F and ROT-H are isomorphous,[21] they may be modeled identically by replacing the appropriate hydrogen atom in ROT-H with a fluorine atom to make ROT-F and thus adding a permanent dipole moment of 1.5 D.

The crystalline environment about a rotor was simulated with two different models, shown in Fig. 4. The local model involves one reference molecule surrounded by six interpenetrating neighbors, which form a crystalline cage within which the central rotary portion can rotate. In the truncated model, only the closest triphenyl groups of the six neighbor molecules are included with hydrogen atoms substituted for the truncated segments. Thus, only a single dipole is considered in this model.

The results obtained using the local model for the desolvated crystal of ROT-F and ROT-H show the expected two-minima potential with 170 deg well separation in ROT-F and 180 deg in ROT-H. For ROT-F, the calculation predicts a well asymmetry of 3.0 kcal/mol while degenerate wells are predicted for ROT-H. The smallest barrier to rotation, E_B, found for ROT-F is 9.8 kcal/mol.

The results of the truncated calculation exhibit no changes in the barrier heights and asymmetry with respect to the local

calculation. Since the truncated model does not account for the rotating parts of the neighboring molecules, the barrier in both the dipolar and nonpolar cases can be completely attributed to steric interactions with nonrotating portions of the crystal lattice. In a separate calculation, long-range electrostatic dipole-dipole interactions between rotors were included using an Ewald-Kornfeld summation[28] and these were found to make a negligible contribution to the rotational potential compared to the steric contribution. This indicates that the rotors may be treated as a dilute and noninteracting collection.

Thus, we have explored thermally driven rotation for a collection of dipolar molecular rotors in a three dimensional crystal. Two environments, a desolvated structure and a clathrate, were studied with dielectric measurements. For both environments, a barrier to rotation of $\sim$13 kcal/mol is observed with a different well asymmetry for each that is much smaller than the barrier. These measurements are in agreement with an examination of the desolvated crystal by ^{2}H NMR. The presence of a two-well asymmetric potential is consistent with the crystal structure, and calculations indicate that the rotational potential is dominated by steric interactions between the dipolar rotor and the trityl groups of neighboring molecules.

Work at the University of Colorado was supported by the U.S. Army Research Office (DAAD19-01-1-0521). Work at UCLA was supported by NSF Grant Nos. DMR-0307028, CHE-9871332 (x ray), and DMR-9975975 (solid state NMR).

*Present address: Dept. of Physics, North Carolina State University, Box 8202, Raleigh, NC 27695, USA.

[1] V. Rozenbaum, V. Ogenko, and A. Chuiko, Sov. Phys. Usp. **34**, 883 (1991).
[2] E. Chacón and P. Tarazona, Phys. Rev. B **39**, 7111 (1989).
[3] K. Kim and N. S. Sullivan, Phys. Rev. B **55**, R664 (1997).
[4] D. Bonart and J. B. Page, Phys. Rev. E **60**, R1134 (1999).
[5] J. de Jonge, M. Ratner, and R. S. S. W. de Leeuw, J. Phys. Chem. B **108**, 2666 (2004).
[6] N. G. McCrum, B. E. Read, and G. Williams, *Anelastic and Dielectric Effects in Polymeric Solids* (Dover, New York, 1991).
[7] G. S. Kottas, L. I. Clarke, D. Horinek, and J. Michl, Chem. Rev. (Washington, D.C.) **105**, 1281 (2005).
[8] J. Ortiz-Lopez, M. S. Li, and F. Luty, Phys. Status Solidi B **199**, 245 (1997).
[9] G. Desiraju, *Crystal Design: Structure and Function, Perspectives in Supramolecular Chemistry* (Wiley, Chichester, 2003), Vol. 7.
[10] A. Gavezzotti, *Theoretical Aspects and Computer Modeling of the Molecular Solid State, The Molecular Solid State* (Wiley, Chichester, 1997), Vol. 1.
[11] S. I. Stupp, V. LeBonheur, K. Walker, L. S. Li, K. Huggins, M. Keser, and A. Amstutz, Science **276**, 384 (1997).
[12] V. A. Russell, C. C. Evans, W. Li, and M. D. Ward, Science **276**, 575 (1997).
[13] G. R. Desiraju, Angew. Chem., Int. Ed. Engl. **34**, 2311 (1995).
[14] J. Dunitz, E. Maverick, and K. N. Trueblood, Angew. Chem., Int. Ed. Engl. **27**, 880 (1988).
[15] L. I. Clarke, D. Horinek, G. S. Kottas, N. Varaska, T. F. Magnera, T. P. Hinderer, R. D. Horansky, J. Michl, and J. C. Price, Nanotechnology **13**, 533 (2002).
[16] J. M. Tour, *Molecular Electronics* (World Scientific, River Edge, 2003).
[17] V. Balzani and M. Venturi, *Molecular Devices and Machines: A Tour Into the Nano World* (Wiley-VCH, Winheim, 2003).
[18] J. Vacek and J. Michl, Proc. Natl. Acad. Sci. U.S.A. **98**, 5481 (2001).
[19] J. Gimzewski, C. Joachim, R. R. Schlittler, V. Langlais, H. Tang, and I. Johannsen, Science **281**, 531 (1998).
[20] Z. Dominguez, H. Dang, M. J. Strouse, and M. A. Garcia-Garibay, J. Am. Chem. Soc. **124**, 7719 (2002).
[21] Z. Dominguez, T.-A. V. Khuong, H. Dang, C. N. Sanrame, J. E. Nunez, and M. A. Garcia-Garibay, J. Am. Chem. Soc. **125**, 8827 (2003).
[22] H. Frohlich, *Theory of Dielectrics* (Clarendon Press, Oxford, 1958).
[23] P. Debye, *Polar Molecules* (The Chemical Catalog Company, New York, 1929).
[24] A. Ronemus, R. Vold, and R. Vold, J. Magn. Reson. (1969-1992) **70**, 416 (1986).
[25] S. Nishikiori, T. Soma, and T. Iwamoto, J. Inclusion Phenom. Mol. Recognit. Chem. **27**, 233 (1997).
[26] N. L. Allinger, Y. H. Yuh, and J.-H. Lii, J. Am. Chem. Soc. **111**, 8551 (1989).
[27] F. Mohamadi, N. Richards, W. C. Guida, R. Liskamp, M. Lipton, C. Caufield, G. Chang, T. Hendrickson, and W. Still, J. Comput. Chem. **11**, 440 (1990).
[28] D. Frankel and B. Smit, *Understanding Molecular Simulation* (Academic Press, San Diego, 2002).
[29] $Q_{CC}=e^2q_{zz}Q/h$, where e and h are the electron charge and Plank constant, respectively, Q is the quadrupole moment of the deuteron, and q_{zz} is the magnitude of the principal component of the electric field gradient tensor (which lies along the C—H bond).